Journal of Nuclear Medicine, published on September 18, 2020 as doi:10.2967/jnumed.120.245084

FAPI-74 PET/CT Using Either ^{18}F-AlF or Cold-kit ^{68}Ga-labeling: Biodistribution, Radiation Dosimetry and Tumor Delineation in Lung Cancer Patients

Frederik L. Giesel[1]* & Sebastian Adeberg[2-5]*, Mustafa Syed[2,4], Thomas Lindner[1], Luis David Jiménez-Franco[6], Eleni Mavriopoulou[1], Fabian Staudinger[1], Eric Tonndorf-Martini[2,4], Sebastian Regnery[2,4], Stefan Rieken[2,5,7], Rami El Shafie[2,5], Manuel Röhrich[1], Paul Flechsig[1], Andreas Kluge[6], Annette Altmann[1], Jürgen Debus[2-5], Uwe Haberkorn[1,8§], Clemens Kratochwil[1]

*Contributed equally to this work.

(1) Department of Nuclear Medicine, University Hospital Heidelberg, Heidelberg Germany
(2) Heidelberg Institute of Radiation Oncology (HIRO), Im Neuenheimer Feld 400, 69120 Heidelberg, Germany
(3) Heidelberg Ion-Beam Therapy Center (HIT), Im Neuenheimer Feld 450, 69120 Heidelberg, Germany
(4) University Hospital Heidelberg, Department of Radiation Oncology, Im Neuenheimer Feld 400, 69120 Heidelberg, Germany
(5) Clinical Cooperation Unit Radiation Oncology, German Cancer Research Center (DKFZ), Im Neuenheimer Feld 280, 69120 Heidelberg, Germany
(6) ABX-CRO advanced pharmaceutical services Forschungsgesellschaft mbH, Dresden, Germany
(7) University Hospital Göttingen, Department of Radiation Oncology, Robert-Koch-Str. 40, 37075 Göttingen, Germany
(8) Clinical Cooperation Unit Nuclear Medicine, German Cancer Research Center (DKFZ), Heidelberg, Germany

§ Corresponding author:
Uwe Haberkorn
Department of Nuclear Medicine
University Hospital Heidelberg
Im Neuenheimer Feld 400
69120 Heidelberg
Tel: +49-6221-56-7732
Fax: +49-6221-56-5288

First author
Frederik L. Giesel
Department of Nuclear Medicine
University Hospital Heidelberg
Im Neuenheimer Feld 400
69120 Heidelberg

Short running title: FAPI-74 biodistribution in patients
Word count: 4800

Abstract

^{68}Ga-FAPI-2/4/46 have already been proposed as promising PET-tracers. However, the short half-life of ^{68}Ga ($T_{1/2}$ 68 min) creates problems with manufacture and delivery. ^{18}F ($T_{1/2}$ 110 min) labeling would result in a more practical large scale production and a cold-kit formulation would improve the spontaneous availability. The NOTA-chelator ligand FAPI-74 can be labeled with both ^{18}F-AlF (Aluminum-Fluoride) and ^{68}Ga. Here we describe the in-vivo evaluation of ^{18}F-FAPI-74 and a proof-of-mechanism of ^{68}Ga-FAPI-74 labeled at ambient temperature. **Methods:** In ten patients with lung cancer PET-scans were acquired at 10 min, 1h and 3h after administration of 259±26 MBq ^{18}F-FAPI-74. Physiological biodistribution and tumor uptake were semi-quantitatively evaluated based on SUV at each time-point. Absorbed doses were evaluated using OLINDA/EXM 1.1 and QDOSE dosimetry software with the dose calculator IDAC-Dose 2.1. Identical methods were used to evaluate one exam after injection of 263 MBq ^{68}Ga-FAPI-74. **Results:** The highest contrast was achieved 1 h p.i. in primary tumors, lymph node and distant metastases with SUVmax >10, respectively. The effective dose per 100 MBq administered activity of ^{18}F-FAPI-74 was 1.4±0.2 mSv and for ^{68}Ga-FAPI-74 it was 1.6 mSv. Thus, the radiation burden of a diagnostic ^{18}F-FAPI-74 PET-scan is even lower than that of PET-scans with ^{18}F-FDG and other ^{18}F-tracers; ^{68}Ga-FAPI-74 is comparable to other ^{68}Ga-ligands. FAPI-PET/CT supported target volume definition for guiding radiotherapy. **Conclusion:** High contrast and low radiation burden of FAPI-74 PET/CT favors multiple clinical applications. Centralized large-scale production of ^{18}F-FAPI-74 or decentralized cold-kit labeling of ^{68}Ga-FAPI-74 allows flexible routine use.

Key words: FAPI PET/CT, cancer associated fibroblasts, lung cancer, radiation dosimetry, cold kit

INTRODUCTION

Fibroblast activation protein (FAP) is highly expressed in the stroma of a variety of human cancers and is therefore, considered promising for guiding targeted therapy *(1)*. Quinoline-based FAP-inhibitors (FAPIs) specifically bind to the enzymatic domain of FAP and are then internalized *(2)*. Methods for conjugation of quinoline-based FAP-ligands with chelators suitable for radiolabeling with various radio-metals were developed *(3,4)*. Labeled with the positron emitter ^{68}Ga, these novel FAP-targeted tracers demonstrated tumor to non-tumor contrast-ratios that were equal or even higher than those attained with FDG-PET/CT *(5)*.

While ^{68}Ga is available via approved ^{68}Ge/^{68}Ga-generators, which allows batch production of approximately 2-3 patient doses per elution, the relatively short half-life of ^{68}Ga ($T_{1/2}$ 68 min, 1.90 MeV positron energy) poses some disadvantages with respect to production capacity and nuclear decay properties. The short half-life mandates in-house production, making delivery to remote centers challenging. In large centers with high patient throughput, several productions per day are required to meet potential demands, occupying a skilled workforce of radiochemists and radiopharmacists over a protracted time period of the work day. If ^{68}Ga-FAPI PET were to replace ^{18}F-FDG PET in clinical routine, multiple generators would be needed, thus multiplying costs. Labeling with ^{18}F ($T_{1/2}$ 110 min, 0.65 MeV positron energy) would solve these issues. Centers with an on-site cyclotron can produce ^{18}F at moderate costs and commercial sites can distribute ^{18}F-labeled compounds over a wide metropolitan area eliminating the need for on-site radiochemistry *(6)*. The lower positron energy of ^{18}F could theoretically improve spatial resolution *(7)*.

As described in a dedicated chemistry/preclinical manuscript (submitted for publication simultaneously), attempts to label FAPIs with covalently attached ^{18}F were initially unsuccessful by demonstrating poor tumor uptake. In contrast, chelation of aluminum fluoride (AlF), an approach that was proposed several years ago and has now been optimized with regard to labeling yield and specific activity *(8)*, presented favorable results in combination with the NOTA-containing FAPI-74. The NOTA-chelator also allows chelation with ^{68}Ga at room temperature, which would also simplify local on-demand production in centers that already own a ^{68}Ge/^{68}Ga-generator.

The aim of this work is to analyze the time dependent tumor-uptake and tracer bio-distribution and to perform absorbed dose estimations for ^{18}F-FAPI-74 PET/CT scans using exams that were done under medical indication to assist tumor volume delineation for guiding radiotherapy in lung cancer patients. In addition we demonstrate proof-of-mechanism for ^{68}Ga-FAPI-74 PET/CT after tracer labeling at ambient temperature.

MATERIALS AND METHODS

Patients

This analysis includes 10 patients (4 male, 6 female) with lung cancer (8 adenocarcinoma, 2 squamous cell carcinoma) and a median age of 65 y (range 45-77 y). All patients gave written informed consent to receive "FAPI-PET/CT" following national regulations and the Declaration of Helsinki. The radiopharmaceutical was produced in accordance to the German Pharmaceuticals Act §13(2b). All patients were referred by a radiation-oncologist, in order to improve tumor delineation for radiotherapy planning of central-pulmonary lesions which would presumable have been challenging to discriminate from the myocardium with ^{18}F-FDG PET. The retrospective evaluation of data acquired under clinical indication was approved by the ethical committee of Heidelberg University (permit S016/2018).

Radiopharmaceuticals

The chemical synthesis of the FAPI-74 precursor and the preclinical evaluation of this tracer are described within a dedicated manuscript (submitted for publication simultaneously).

Chelation with ^{18}F-AlF were performed following McBride et al. (*8*) as follows: 2-10 GBq ^{18}F fluoride (ZAG Cyclotron AG, Karlsruhe, Germany) in 4 mL water were trapped on an anion exchange cartridge (Waters Accel Plus QMA Light cartridge, preconditioned with 5 mL 0.5 M NaOAc pH 3.9 and 10 mL of water) and eluted with 0.30 mL 0.5 M NaOAc pH 3.9. The solution was incubated with 6 µL of AlCl3 in water (10 mM) and 300 µL dimethyl sulfoxide (DMSO, Simga-Aldrich, Darmstadt, Germany) for 5 min at room temperature before 20 µL of a solution of FAPI-74 (4 mM) were added. The reaction was carried out at 95 °C for 15 min, cooled to room temperature, diluted with 5 mL water and worked up by SPE (Waters Oasis HLB Plus Light cartridge). The final product was eluted with 0.5 mL ethanol, 5 mL 0.9% saline and spiked with phosphate buffer before sterile filtration (Filtropur S 0.2; Sarstedt).

Chelation with ^{68}Ga was achieved by adding 1.00 mL ^{68}Ge/^{68}Ga-generator eluate (0.6 M hydrochloric adic; ca. 1.2 GBq) to a mixture of 15 µL FAPI-74 solution (4 mM in water), 310 µL sodium acetate (2.5 M in water) and 0.50 mL ethanol. After incubation for 15 min at room temperature the reaction was worked up by SPE as described for ^{18}F-FAPI-74.

PET/CT Imaging

All imaging was performed on a Biograph mCT Flow scanner (Siemens, Erlangen, Germany). PET was acquired in 3-D mode (matrix 200 × 200) using FlowMotion (Siemens). The emission data was corrected for randoms, scatter and decay. Reconstruction was performed with an ordered subset expectation maximization (OSEM) algorithm with two iterations/21 subsets and Gauss-filtered to a transaxial resolution

of 5 mm at full-width at half-maximum (FWHM); attenuation correction was performed using the unenhanced low-dose CT images. The CT-scans were reconstructed to a slice thickness of 5 mm, increment of 3 mm, soft tissue reconstruction kernel (B30), using CareDose (Siemens). All patients were imaged at 10 min, 1h and 3h after injection of either 259±26 MBq (198-290 MBq) ^{18}F-FAPI-74 in ten or 263 MBq ^{68}Ga-FAPI-74 in one patient.

FAPI-Based Target Volume of Primary Tumors

The acquired ^{18}F-FAPI-74 PET/CT exams were used to assist tumor volume delineation for guiding radiotherapy in patients with lung cancer, similar to previous use of ^{18}F-FDG PET/CT (*9,10*). Target volume definition was done using Siemens Syngo.via software (Siemens, Erlangen, Germany). CT-based GTVs were contoured on soft-tissue and lung windows using contrast-enhanced exams. PET-based GTVs (FAPI-GTV) were assessed comparing tumor SUVs to healthy surrounding tissue using Syngo's auto-contour algorithm at various SUV thresholds. Two segmentation approaches were considered: either x-fold of background or percentage of SUVmax. Contours were manually adjusted, checked for plausibility and corrected for false positive/negative uptake by two experienced radiation oncologists and two nuclear medicine physicians, board-certified respectively. In clinical practice, radiation field definition is inherently a subjective task and so consensus of expert readers is usually considered the best applicable standard of reference.

Biodistribution

For calculation of the standardized uptake value (SUV), circular regions of interest were drawn around the tumor lesions with focally increased uptake in transaxial slices and automatically adapted to a three-dimensional volume-of-interest (VOI) with e.soft software (Siemens) at a 40 % isocontour. The tracer biodistribution in patients was quantified by SUVmean and SUVmax at 10 min, 1 h and 3h post injection of ^{18}F-FAPI-74. The normal organs (brain, oral mucosa, parotid, thyroid, lung, heart muscle, aortic lumen content, liver, pancreas, spleen, kidney, colon, muscle, fat and spinal cord) were evaluated with a 2 cm sphere placed inside the organ parenchyma. Statistical analysis and graphic output where performed with SigmaPlot.

Radiation Dosimetry Estimate

The dosimetry analysis was performed using the QDOSE dosimetry software suite v1.1.4 (ABX-CRO, Dresden, Germany).

After all PET and corresponding CT data were imported into the QDOSE software, CT images were coregistered using an automatic rigid coregistration algorithm. PET images were coupled to the CT of the corresponding imaging time-point and manually coregistered to this CT when necessary. The frame acquisition time was adjusted from the start of the scan (standard for DICOM-header) to the middle of the acquisition frame (difference of 9.6 min ± 1.2 min), which appears more appropriate for pharmacokinetic evaluation.

Kidneys, liver, spleen, urinary bladder content, red marrow, heart content and remainder body were considered as source organs. According to an established model, the red marrow activity was approximated by extrapolating activity retrieved from VOIs in the lumbar vertebrae 1-5 (approx. 12.3% of the red-marrow space) to the total red-marrow *(11)*.

As limbs were cropped by the limited field of view of the PET-scan, the total body cumulated activity ($\tilde{A}_{Total\_Body}$), which is important to determine the cumulated activity in the remainder body for dose calculations, was estimated using the injected activity (A) and the effective half-life (T_{eff}) of a VOI covering the majority of the body. Thus, the total body cumulated activity was calculated as:

$$\tilde{A}_{Total\_Body} = (A \cdot T_{eff})/(Ln(2))$$

For segmentation of the source organs, VOIs were defined for the kidneys (left and right), liver, spleen, urinary bladder, heart, lumbar vertebrae (LV1 to LV5) and total body. Tumor areas were not considered in the segmented VOIs. Each source organ was manually segmented on the PET images in each time-point and activity values were retrieved to determine the time-activity curves (TACs) for the organs. The volumes of the liver, kidneys and spleen were determined from segmentation in the CT images. The calculation of the masses (assuming a density of 1.06 g/mL) was automatically performed in QDOSE based on the segmented VOIs in the CT images.

The TAC for the kidneys was automatically calculated as the sum of the activities in the left and right kidneys. Mono-exponential curve fitting was then applied to all organ TACs. The fitted TACs were then integrated from time 0 min to infinity to obtain the cumulated time-activity (Ã) values. The Ã values of the total body and red marrow were added as additional organs into QDOSE as external calculations for these organs were performed. The Ã of the remainder body was automatically calculated by subtracting the Ã of all source organs from the total body Ã. Residence times were calculated by dividing the Ã of each source organ by the injected activity and further exported to OLINDA/EXM v1.1 *(12)* for dose calculation with this software.

Absorbed and effective dose calculations were performed using OLINDA/EXM 1.1 *(12)* with the residence times exported from QDOSE. In addition, the IDAC-Dose 2.1 dose calculator *(13)* integrated in QDOSE was also used to perform dose estimations. IDAC-Dose 2.1 is based on the adult reference computational phantoms of the international commission on radiological protection (ICRP) *(14)* and on the ICRP specific absorbed fractions *(15)*. Organ masses for the kidneys, liver and spleen, obtained from the

segmentation in the CT images, were individually adapted for each patient both in QDOSE (using IDAC-Dose 2.1) and in OLINDA/EXM to obtain more accurate dose estimations.

RESULTS

Adverse Events

The mean administered activity of ^{18}F-FAPI-74 was 259±26 MBq (range 198-290 MBq); for the ^{68}Ga-FAPI-74 exam it was 263 MBq. After quality control, the specific activities of ^{18}F-FAPI-74 were 20-50 nmol/GBq (equals 14.7-36.8 µg/GBq); the specific activity of ^{68}Ga-FAPI-74 was ~100 nmol/GBq (73.6 µg/GBq) and only moderately worsened by physical decay during the short delay between on-site labeling and injection. Thus, the administered masses of FAPI-74 (735.8 g/mol) were about 5-40 µg per patient-dose. All patients tolerated the examination well. No drug-related pharmacological effects or physiologic responses occurred. All observed parameters remained normal and unchanged during and after the examination. No patient reported subjective symptoms during the 3.5 h observation period after tracer injection.

Normal-organ Biodistribution and Tumor Uptake

The biodistribution of ^{18}F-FAPI-74 in normal organs and tumor is presented in Fig.-1 and illustrated as time-dependent maximum-intensity-projections in Fig.-2. In contrast to the previous ^{68}Ga-FAPI-2/4 *(5)*, the oral mucosa uptake does not exceed the background in muscle and connective tissue. Another difference is a moderately higher blood-pool, both on the initial and delayed imaging. There was no difference between blood-pool and muscle uptake with ^{68}Ga-FAPI-2/4, but with ^{18}F-FAPI-74 vessels are definable at all time-points. According to our previous FAPI-tracers, there was no uptake of ^{18}F-FAPI-74 in the liver or spleen exceeding the perfusion dependent background. Within this small sample size, the tumor-uptake of adeno vs. squamous-cell carcinoma showed no difference nor was it different in comparison to previous results with ^{68}Ga-FAPI-4 *(16)*. In primary lung tumors the average SUVmax was 11.8 at 10 min; 12.7 at 1h and 11.3 at 3h p.i. Lymph node metastases had SUVmax of 9.9 at 10 min, 10.7 at 1h and 9.4 at 3h. Distant metastases demonstrated an average SUVmax of 11.8 at 10 min, 11.8 at 1h and 11.4 at 3h, respectively. Therefore, the uptake generally peaks later than 10 min p.i. but there is already some wash-out from tumor tissue between 1h and 3h p.i.; therefore the best contrast between tumor and background is achieved at 1h p.i. and this time-point was consecutively used to evaluate gross-tumor-volume (GTV) delineation for guiding radiotherapy. The one patient receiving ^{68}Ga-FAPI-74 is presented in Fig.-3 and presents a similar kinetics, with tumor SUVmax of 10.4 at 10 min, 11.4 at 1 h and 8.7 at 3h.

Automated Target Volume Delineation of FAPI GTVs

Contouring primary lung tumors on CT resulted in a median GTV of 67.4mL (range 25.9-343.4mL). Using a cut-off at 3-fold background, the ^{18}F-FAPI-74 PET traced a median GTV of 69.8mL ($p = 0.21$; range: 5.0-527.0 mL); Fig.-4. With background SUVs of approx. 2 and tumor SUVs of approx. 12, this is widely comparable to a cut-off at 40-50% SUVmax. In consensus with the radiation-oncologist, these PET-segmented volumes were considered more likely to reflect actual tumor volumes than the corresponding CT. One patient that was initially considered oligo-metastatic per CT, was up-staged and consecutively transferred to chemotherapy after additional tumor lesions were found on ^{18}F-FAPI-74 PET imaging (Fig.-2).

Radiation Dosimetry

The OLINDA/EXM-based dosimetry estimates are presented in Table 1. Calculations according to the IDAC-Dose 2.1 dose calculator are presented in the Supplemental-Table. For ^{18}F-FAPI-74 the normalized effective dose was 1.4±0.2 mSv / 100 MBq (range 1.1-1.7 mSv / 100 MBq) with OLINDA/EXM and 1.2±0.1 mSv / 100 MBq (range 1.0-1.4 mSv / 100 MBq) with IDAC-Dose 2.1. Thus, the exams, which were conducted with 198-290 MBq ^{18}F-FAPI-74 translated into effective doses of approx. 3-4 mSv per exam based on the OLINDA/EXM mean effective dose. For ^{68}Ga-FAPI-74 the effective dose was 1.6 mSv / 100 MBq with OLINDA/EXM and 1.4 mSv / 100 MBq with IDAC-2.1. Due to a rapid renal tracer clearance and low nonspecific uptake in normal organs, the radiation dosimetry estimate of ^{18}F-FAPI-74 compares favorably to most other ^{18}F-labeled PET-tracers in clinical use, while ^{68}Ga-FAPI-74 is in the same range as other ^{68}Ga-labeled tracers including FAPI-2/4/46 (Table 2).

DISCUSSION

In this work we evaluated the biodistribution and radiation-dosimetry of ^{18}F-FAPI-74 PET and demonstrated its possible value for guiding radiotherapy. In addition labeling of ^{68}Ga-FAPI-74 at ambient temperature was established and its in-vivo performance was evaluated using identical methods.

Based on the time-dependent biodistribution of ^{68}Ga- and ^{18}F-FAPI-74 in tumor and normal organs, optimal tumor to background ratios at limited noise was achieved by image acquisition 1h post injection. This is in contrast to previous experience with ^{68}Ga-FAPI-2/4, for which no improvement in tumor uptake between 10 min and 1h p.i. was observed. In normal organs the time-dependent biodistribution was nearly identical to other quinoline-based FAPIs (*5*).

With a mean normalized effective dose of 1.4 mSv per 100 MBq (3.5 mSv for a typical 250 MBq exam), the radiation burden of an ^{18}F-FAPI-74 PET is lower than that of PET-scans with ^{18}F-FDG, the current standard in oncologic imaging (Table 2). The faint physiological cerebral and hepatic uptake of ^{18}F-FAPI-

74 likely accounts for a lower radiation exposure. The effective dose of 1.6 mSv per 100 MBq (3.0 mSv for a typical 185 MBq exam) of a ^{68}Ga-FAPI-74 PET scan is within the range for PET imaging with ^{68}Ga-FAPI-2/4/46, which is well expected as all of them share a very similar biodistribution and tracer kinetics.

We used ^{18}F-FAPI-74 PET/CT to plan radiotherapy in patients with lung cancer. Currently, ^{18}F-FDG PET/CT is the standard for staging and target volume delineation in lung cancer. With ^{18}F-FDG PET/CT it is possible to identify additional distant metastases in approx. 5-30% of patients *(17)* and its high sensitivity for mediastinal lymph nodes of 90-100% is considered sufficient to limit the target volume to involved regions. The specificity of ^{18}F-FDG PET/CT is approx. 80% due to false positive findings (*18-24*). Our preliminary experience in 11 patients is not sufficient to calculate sensitivity, specificity and accuracy of ^{18}F-FAPI-74 PET/CT, yet. However, similar to ^{18}F-FDG PET, with ^{18}F-FAPI-74 PET it was possible to identify additional distant metastases compared to a diagnostic CT (Fig.-2). In a recent case-report, due to its low physiological cerebral background, with ^{68}Ga-FAPI-4 PET/CT it was possible to identify brain metastases from lung cancer (*25*). Thus, the oncological application of ^{18}F-FAPI-74 PET/CT appears promising. By applying various cut-off values, the best correlation between CT and ^{18}F-FAPI-74 PET guided GTV-segmentation was found at uptakes that were 3-fold the background, which equals 40-50% of SUVmax (Fig.-4). This perfectly corresponds to several publications about ^{18}F-FDG PET, which recommends delineating the 3D metabolic target volume at 41-50% of SUVmax *(26-29)*.

Based on the first DOTA modified tracer FAPI-2, the derivatives FAPI-4 and FAPI-46 were developed with a focus on the therapeutic option. The NOTA-derivative FAPI-74 was developed as an exclusive diagnostic ligand, accepting slightly shorter tumor retention than the previous theranostic agents. Nevertheless, at early imaging time-points the diagnostic performance should be very similar. Well in line with our expectations, the tumor SUVs of ^{68}Ga-/ ^{18}F-FAPI-74 are almost equal to FAPI-4, when comparing lung cancer patients, respectively (*16*). In a recent investigation, the accuracy of FAPI-4 PET/CT was directly compared to FDG-PET/CT and favorable tumor-to-background contrast and higher detection rate of primary tumors, lymph-node and visceral metastases of FAPI-PET compared to FDG-PET was found, respectively. In this study histopathology of biopsy or surgical specimens served as the gold standard for the final patients's classification (*30*). In addition to its oncological application, "FAPI-PET" was also found promising to evaluate immune-related and heart diseases (*31,32*). As a practical (i.e. independent from blood-sugar and physical activity), multi-purpose tracer, production capacities could become a relevant issue soon. One additional advantage of FAPI-74 over previous ligands is its preferable suitability for labeling with ^{18}F-AlF, which would allow large-scale batch production and distribution via satellite-concepts. Another characteristic of the NOTA-chelator in FAPI-74 is the possibility for ^{68}Ga-labeling at ambient temperature. Standardized cold-kits would allow charge-wise constancy tests as required by regulatory bodies and would increase the flexibility for local on-demand production using approved ^{68}Ge/^{68}Ga-generators. Thus, in our center, we consider FAPI-74 as the final evolution stage of diagnostic FAP-targeted ligands.

Appropriate approximation of the radiation dosimetry of a novel radiopharmaceutical is mandatory in advance of preparing prospective clinical trials and this investigation is focused on high methodical standards of the dosimetry part, e.g. considering individually segmented organ masses for all patients, respectively. Yet, only few investigations directly comparing ^{68}Ga-FAPI-2/4 versus ^{18}F-FDG with histopathological correlation have been reported (*5,30*). With the still limited patient numbers available until now, the accuracy of FAPI-PET/CT appears promising. However, additional research evaluating the clinical impact of FAPI-PET/CT for particular clinical indications, compared with a reliable standard of truth and including sufficient patient numbers, is still pivotal.

CONCLUSION

The high contrast and low radiation burden of ^{68}Ga-/ ^{18}F-FAPI-74 PET/CT favors multiple clinical applications. Centralized large-scale ^{18}F-AlF based production of ^{18}F-FAPI-74 or decentralized cold-kit labeling of ^{68}Ga-FAPI-74 allows flexible routine use.

ACKNOWLEDGEMENT

We thank Peter L. Choyke from the NIH/NCI molecular imaging program for proof reading and scientific advice. We thank the technical assistants of the PET/CT-group Heidelberg University Hospital for performing the PET-scans.

DISCLOSURE

UH, AL, TL WM, CK, FLG have a patent application for quinolone based FAP-targeting agents for imaging and therapy in nuclear medicine. UH, TL, CK, FLG also have shares of a consultancy-group for iTheranostics. FLG is medical advisor for ABX advanced biochemical compound and Telix Pharmaceuticals. SA and JD received grants from Accuray International Sàrl, Merck Serono GmbH and Astra Zeneca GmbH outside the submitted work. SA received grants from Novocure outside the submitted work. JD received grants from CRI – The Clinical Research Institue GmbH, View Ray Inc., Accuray Incorporated, RaySearch Laboratories AB, Vision RT limited, Astellas Pharma GmbH, Solution Akademie GmbH, Ergomed PLC Surrey Research Park, Siemens Healthcare GmbH, Quintiles GmbH, Pharmaceutical Research Associates GmbH, Boehringer Ingelheim Pharma GmbH Co, PTW-Freiburg Dr. Pychlau GmbH, Nanobiotix A.A. outside the submitted work.
The other authors declare no conflict of interest.

Key Points

QUESTION: To characterize a FAPI variant, that can be used for both ^{18}F- and ^{68}Ga-labelling, with respect to biodistribution and dosimetry.

PERTINENT FINDINGS: The NOTA-chelator within the novel ligand FAPI-74 allows labelling with ^{18}F-AlF as well as the design of a cold kit for labelling with ^{68}Ga. In patients with lung cancer the new ligands presented similar performance and radiation dosimetry than previous FAPIs.

IMPLICATIONS FOR PATIENT CARE: FAPI-74 is our final stage PET-tracer for imaging of Fibroblast Activating Protein in-vivo.

REFERENCES

1. Brennen WN, Isaacs JT, Denmeade SR. Rationale behind targeting fibroblast activation protein-expressing carcinoma-associated fibroblasts as a novel chemotherapeutic strategy. *Mol Cancer Ther.* 2012;11:257-266.
2. Jansen K, Heirbaut L, Cheng JD, et al. Selective inhibitors of fibroblast activation protein (FAP) with a (4-quinolinoyl)-glycyl-2-cyanopyrrolidine scaffold. *ACS Med Chem Lett.* 2013;4:491-496.
3. Lindner T, Loktev A, Altmann A, et al. Development of quinoline-based theranostic ligands for the targeting of fibroblast activation protein. *J Nucl Med.* 2018;59:1415-1422.
4. Loktev A, Lindner T, Mier W, et al. A tumor-Imaging method targeting cancer-associated fibroblasts. *J Nucl Med.* 2018;59:1423-1429.
5. Giesel FL, Kratochwil C, Lindner T, et al. (68)Ga-FAPI PET/CT: Biodistribution and preliminary dosimetry estimate of 2 DOTA-Containing FAP-targeting agents in patients with various cancers. *J Nucl Med.* 2019;60:386-392.
6. Kesch C, Kratochwil C, Mier W, et al. (68)Ga or (18)F for prostate cancer imaging? *J Nucl Med*. 2017;58:687-688
7. Sanchez-Crespo A. Comparison of gallium-68 and fluorine-18 imaging characteristics in positron emission tomography. Appl Radiat Isot 76:55-62, 2013
8. McBride WJ, Sharkey RM, Karacay H, et al. A novel method of 18F radiolabeling for PET. *J Nucl Med.* 2009;50:991–998.
9. Paulino AC, Johnstone PA. FDG-PET in radiotherapy treatment planning: pandora's box? *Int J Radiat Oncol Biol Phys.* 2004;59:4-5.
10. Nestle U, Schaefer-Schuler A, Kremp S, et al. Target volume definition for 18F-FDG PET-positive lymph nodes in radiotherapy of patients with non-small cell lung cancer. *Eur J Nucl Med Mol Imaging.* 2007;34:453-462.
11. Hindorf C, Glatting G, Chiesa C, et al. EANM Dosimetry committee guidelines for bone marrow and whole-body dosimetry. *Eur J Nucl Med Mol Imaging.* 2010;37:1238-1250.
12. Stabin MG, Sparks RB, Crowe E. OLINDA/EXM: the second-generation personal computer software for internal dose assessment in nuclear medicine. *J Nucl Med.* 2005;46:1023-1027.
13. Andersson M, Johansson L, Eckerman K, et al. IDAC-Dose 2.1, an internal dosimetry program for diagnostic nuclear medicine based on the ICRP adult reference voxel phantoms. *EJNMMI Res.* 2017;7:88.
14. Menzel HG, Clement C, DeLuca P. ICRP Publication 110. Realistic reference phantoms: an ICRP/ICRU joint effort. A report of adult reference computational phantoms. *Ann ICRP.* 2009;39:1-164.
15. Bolch WE, Jokisch D, Zankl M, et al. ICRP Publication 133: The ICRP computational framework for internal dose assessment for reference adults: specific absorbed fractions. *Ann ICRP.* 2016;45:5-73.
16. Kratochwil C, Flechsig P, Lindner T et al. 68Ga-FAPI PET/CT: Tracer uptake in 28 Different Kinds of Cancer. *J Nucl Med.* 2019;60:801-805.

17. Sahiner I, Vural GU. Positron emission tomography/computerized tomography in lung cancer. *Quant Imaging Med Surg.* 2014;4:195-206.
18. Gould MK, Maclean CC, Kuschner WG, et al. Accuracy of positron emission tomography for diagnosis of pulmonary nodules and mass lesions: a meta-analysis. *JAMA.* 2001;285:914-924.
19. Behzadi A, Ung Y, Lowe V, et al. The role of positron emission tomography in the management of non-small cell lung cancer. *Can J Surg.* 2009;52:235-242.
20. Fernandes AT, Shen J, Finlay J, et al. Elective nodal irradiation (ENI) vs. involved field radiotherapy (IFRT) for locally advanced non-small cell lung cancer (NSCLC): A comparative analysis of toxicities and clinical outcomes. *Radiother Oncol.* 2010;95:178-184.
21. Goldstraw P, Ball D, Jett JR, et al. Non-small-cell lung cancer. *Lancet.* 2011;378:1727-1740.
22. De Ruysscher D, Nestle U, Jeraj R, et al. PET scans in radiotherapy planning of lung cancer. *Lung Cancer.* 2012;75:141-145.
23. Broderick SR, Patterson GA. Performance of integrated positron emission tomography/computed tomography for mediastinal nodal staging in non-small cell lung carcinoma. *Thorac Surg Clin.* 2013;23:193-198.
24. De Ruysscher D. PET-CT in radiotherapy for lung cancer. *Methods Mol Biol.* 2011;727:53-58.
25. Giesel FL, Heussel CP, Lindner T, et al. FAPI-PET/CT improves staging in a lung cancer patient with cerebral metastasis. *Eur J Nucl Med Mol Imaging* 2019;46:1754-1755.
26. Nestle U, Kremp S, Schaefer-Schuler A, et al. Comparison of different methods for delineation of 18F-FDG PET-positive tissue for target volume definition in radiotherapy of patients with non-Small cell lung cancer. *J Nucl Med.* 2005;46:1342-1348.
27. Erdi YE, Mawlawi O, Larson SM, et al. Segmentation of lung lesion volume by adaptive positron emission tomography image thresholding. *Cancer.* 1997;80:2505-2509.
28. Boellaard R, Krak NC, Hoekstra OS, et al. Effects of noise, image resolution, and ROI definition on the accuracy of standard uptake values: a simulation study. *J Nucl Med.* 2004;45:1519-1527.
29. Krak NC, Boellaard R, Hoekstra OS, et al. Effects of ROI definition and reconstruction method on quantitative outcome and applicability in a response monitoring trial. *Eur J Nucl Med Mol Imaging*. 2005;32:294-301.
30. Chen H, Pang Y, Wu J, Zhao L, Hao B et al. Comparison of [68Ga]Ga-DOTA-FAPI-04 and [18F] FDG PET/CT for the diagnosis of primary and metastatic lesions in patients with various types of cancer. Eur J Nucl Med Mol Imaging. 2020 Mar 28. doi: 10.1007/s00259-020-04769-z.
31. Luo Y, Pan Q, Zhang W. IgG4-related disease revealed by 68Ga-FAPI and 18F-FDG PET/CT. *Eur J Nucl Med Mol Imaging.* 2019;46:2625-2626.
32. Varasteh Z, Mohanta S, Robu S, et al. Molecular imaging of fibroblast activity after myocardial infarction using a 68Ga-Labeled fibroblast activation protein inhibitor, FAPI-04. *J Nucl Med.* 2019;60:1743-1749.
33. Meyer C, Dahlbom M, Lindner T, et al. Radiation dosimetry and biodistribution of 68Ga-FAPI-46 PET imaging in cancer patients. *J Nucl Med.* December 13, 2019 [Epub ahead of print]

34. Afshar-Oromieh A, Hetzheim H, Kübler W, et al. Radiation dosimetry of (68)Ga-PSMA-11 (HBED-CC) and preliminary evaluation of optimal imaging timing. *Eur J Nucl Med Mol Imaging.* 2016;43:1611-1620.
35. Sandström M, Velikyan I, Garske-Román U, et al. Comparative biodistribution and radiation dosimetry of 68Ga-DOTATOC and 68Ga-DOTATATE in patients with neuroendocrine tumors. *J Nucl Med.* 2013;54:1755-1759.
36. Quinn B, Dauer Z, Pandit-Taskar N, Schoder H, Dauer LT. Radiation dosimetry of 18F-FDG PET/CT: incorporating exam-specific parameters in dose estimates. *BMC Med Imaging.* 2016;16:41.
37. Vesselle H, Grierson J, Peterson LM, Muzi M, Mankoff DA, Krohn KA. 18F-Fluorothymidine radiation dosimetry in human PET imaging studies. *J Nucl Med.* 2003;44:1482-1488.
38. Pauleit D, Floeth F, Herzog H, et al. Whole-body distribution and dosimetry of O-(2-[18F]fluoroethyl)-L-tyrosine. *Eur J Nucl Med Mol Imaging.* 2003;30:519-524.
39. Smolarz K, Krause BJ, Graner FP, et al. (S)-4-(3-18F-fluoropropyl)-L-glutamic acid: an 18F-labeled tumor-specific probe for PET/CT imaging--dosimetry. *J Nucl Med.* 2013;54:861-866.
40. Giesel FL, Hadaschik B, Cardinale J, et al. F-18 labelled PSMA-1007: biodistribution, radiation dosimetry and histopathological validation of tumor lesions in prostate cancer patients. *Eur J Nucl Med Mol Imaging.* 2017;44:678-688.
41. O'Keefe GJ, Saunder TH, Ng S, et al. Radiation dosimetry of beta-amyloid tracers 11C-PiB and 18F-BAY94-9172. *J Nucl Med.* 2009;50:309-315.
42. Maddahi J, Bengel F, Czernin J, et al. Dosimetry, biodistribution, and safety of flurpiridaz F18 in healthy subjects undergoing rest and exercise or pharmacological stress PET myocardial perfusion imaging. *J Nucl Cardiol.* 2019;26:2018-2030.
43. DeGrado TR, Reiman RE, Price DT, Wang S, Coleman RE. Pharmacokinetics and radiation dosimetry of 18F-fluorocholine. *J Nucl Med.* 2002;43:92-96.
44. Graham MM, Peterson LM, Link JM, et al. Fluorine-18-fluoromisonidazole radiation dosimetry in imaging studies. *J Nucl Med.* 1997;38:1631-1636.

Figures and Legends

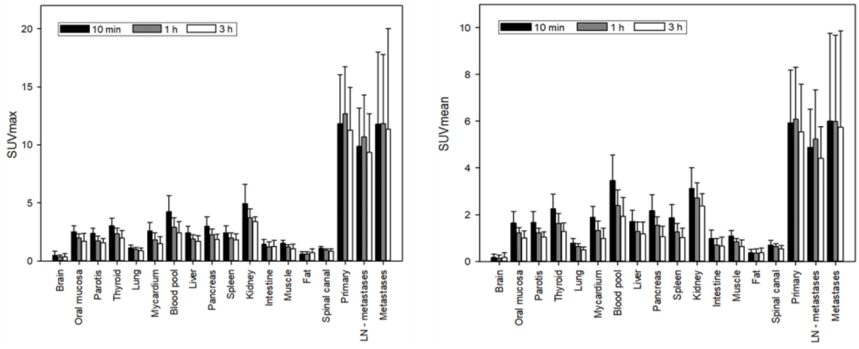

FIGURE 1. Time-dependent bio-distribution of ^{18}F-FAPI-74 in normal organs and tumor

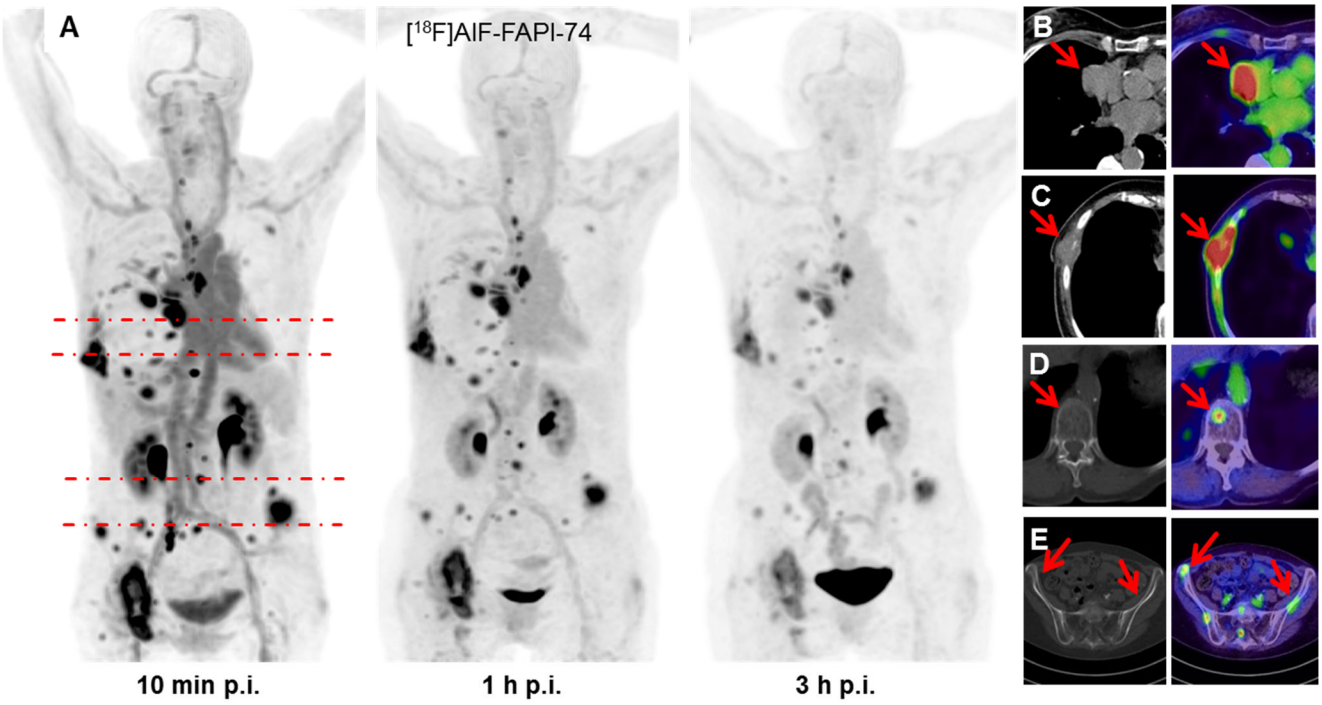

FIGURE 2. Maximum-intensity-projections of ^{18}F-FAPI-74 PET at 10 min, 1 h and 3 h p.i. (A). FAPI-PET/CT presents favorable discrimination between tumor and myocardium (B). Some FAPI-positive lesions were confirmed by CT-correlate (C), while additional bone lesions were only detected per FAPI-PET (D, E).

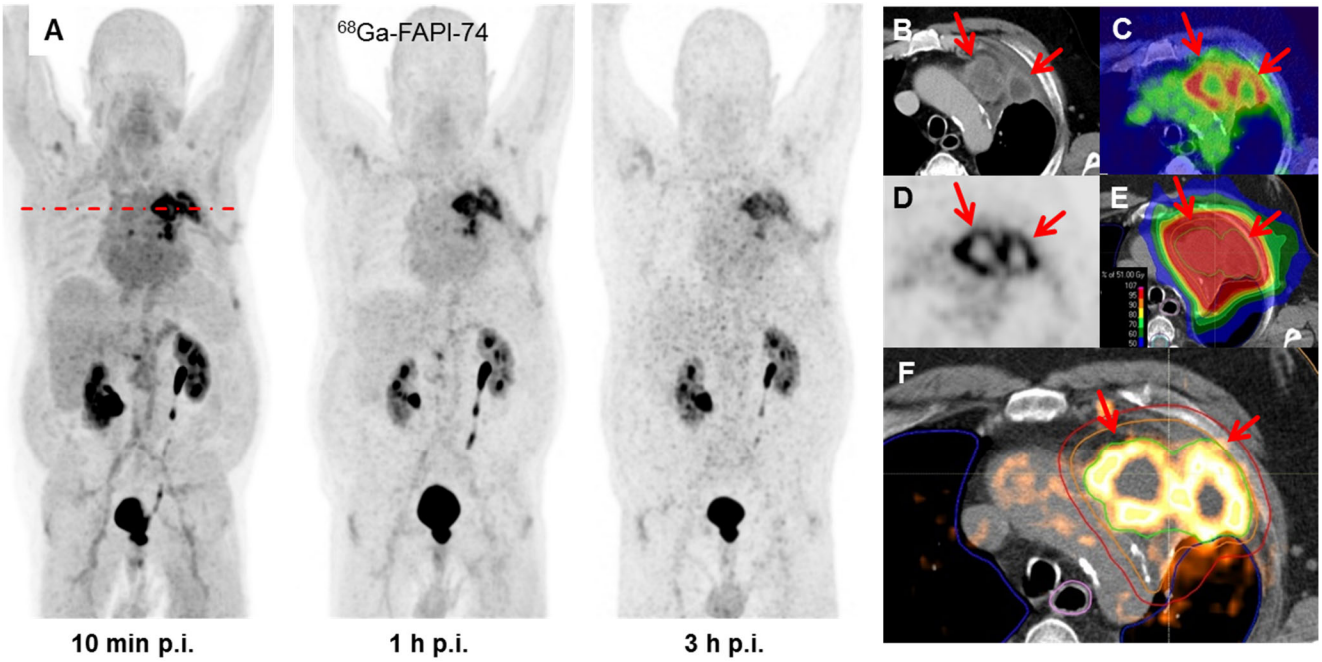

FIGURE 3. Maximum-intensity-projections of ^{68}Ga-FAPI-74 PET at 10 min, 1 h and 3 h p.i. (A). Direct comparison of contrast enhanced CT (B), FAPI-PET (D) and Fusion (C). Superior tumor delineation consecutively improved dose application to tumor volume using a volumetric-modulated arc therapy (VMAT); green line: gross-tumor volume (GTV); orange line: clinical target volume (CTV); red line: planning target volume (PTV) (E, F).

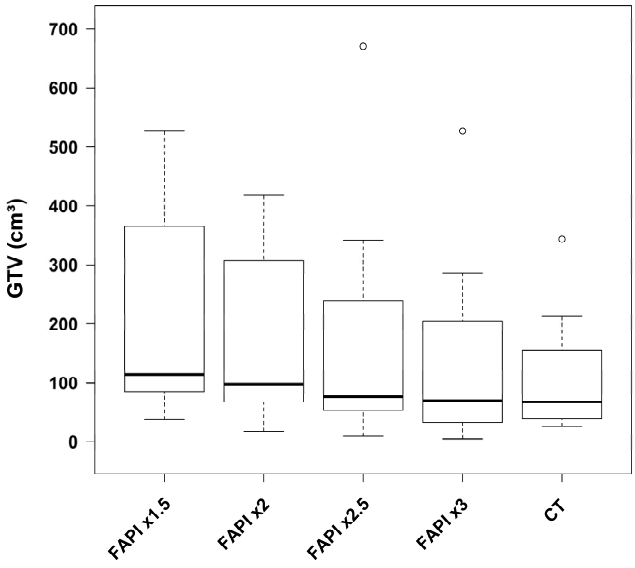

FIGURE 4. Gross-tumor-volume (GTV) automatically segmented per FAPI-PET at different SUV-thresholds (x-fold blood-pool) in comparison to the CT based standard of reference.

Tables

TABLE 1. Dose estimates for ^{18}F- and ^{68}Ga-FAPI-74 according to OLINDA/EXM 1.1

	^{18}F-FAPI-74		**^{68}Ga-FAPI-74**
	N = 10 (mean)		**N = 1**
Target Organ	Absorbed Dose (mSv / 100-MBq)	+/- SD	Absorbed Dose (mSv / 100-MBq)
Adrenals	1.15	0.09	1.29
Brain	0.78	0.09	1.05
Breasts	0.78	0.07	1.04
Gallbladder Wall	1.17	0.10	1.33
LLI Wall	1.23	0.16	1.31
Small Intestine	1.16	0.12	1.29
Stomach Wall	1.06	0.10	1.24
ULI Wall	1.13	0.11	1.27
Heart Wall	2.29	0.28	3.40
Kidneys	2.94	0.79	3.51
Liver	1.50	0.36	1.33
Lungs	0.96	0.07	1.16
Muscle	0.94	0.10	1.14
Ovaries	1.25	0.16	1.33
Pancreas	1.18	0.10	1.32
Red Marrow	1.12	0.11	1.11
Osteogenic Cells	1.53	0.14	1.70
Skin	0.73	0.08	1.00
Spleen	1.67	0.44	1.19
Testes	0.99	0.13	1.16
Thymus	1.02	0.09	1.21
Thyroid	0.91	0.09	1.13
Urinary Bladder Wall	7.58	2.84	9.86
Uterus	1.49	0.25	1.46
Total Body	0.97	0.09	1.22
Effektive Dose	**1.41**	0.22	**1.61**

TABLE 2 Effective dose of ^{18}F-FAPI-74 and ^{68}Ga-FAPI-74 in comparison to other PET-tracers

PET-Tracer	Effective Dose (mSv / MBq)	Reference
^{18}F-FAPI-74	0.014	this work
^{68}Ga-FAPI-74	0.016	this work
^{68}Ga-FAPI-2/4/46	0.008-0.015	(*5,33*)
^{68}Ga-PSMA-11	0.023	(*34*)
^{68}Ga-DOTATOC/-TATE	0.021	(*35*)
^{18}F-FDG	0.020	(*36*)
^{18}F-FLT	0.028	(*37*)
^{18}F-FET	0.016	(*38*)
^{18}F-FSPG	0.032	(*39*)
^{18}F-PSMA-1007	0.022	(*40*)
^{18}F-Flurbetaben	0.015	(*41*)
^{18}F-Flurpiridaz	0.019	(*42*)
^{18}F-Fluorocholine	0.031	(*43*)
^{18}F-MISO	0.013	(*44*)

SUPPLEMENT

SUPPLEMENTAL-TABLE. Dose estimates for ^{18}F- and ^{68}Ga-FAPI-74 according to IDAC-Dose 2.1

	^{18}F-FAPI-74		^{68}Ga-FAPI-74
	N = 10 (mean)		N = 1
Target Organ	Absorbed Dose (mSv / 100-MBq)	+/- SD	Absorbed Dose (mSv / 100-MBq)
Adipose	**0,95**	0,10	**1.24**
Adrenals	**1,34**	0,10	**1.59**
Alveolar-interstitium	**0,74**	0,07	**0.82**
Brain	**0,86**	0,08	**1.17**
Breasts	**0,78**	0,07	**1.10**
Bronchial bound region	**0,89**	0,08	**1.00**
Bronchial sequestered re	**0,89**	0,08	**0.99**
Bronchiolar sequestered	**0,76**	0,07	**0.86**
Colon	**1,03**	0,11	**1.01**
Cortical bone mineral su	**0,83**	0,08	**0.95**
ET region	**0,62**	0,06	**0.72**
ET1 surface	**0,41**	0,04	**0.51**
ET2 surface	**0,62**	0,06	**0.72**
Extrathoracic lymph nod	**0,95**	0,09	**1.27**
Eye lenses	**0,65**	0,06	**0.71**
Gallbladder wall	**1,16**	0,12	**1.39**
Heart wall	**0,95**	0,08	**1.26**
Kidneys	**2,97**	0,72	**3.46**
Left colon wall	**0,90**	0,08	**0.94**
Liver	**1,40**	0,32	**1.37**
Lungs	**0,80**	0,07	**0.89**
Lymphatic nodes	**1,10**	0,12	**1.34**
Muscle	**0,95**	0,09	**1.24**
Oesophagus wall	**0,93**	0,08	**1.06**
Oral mucosa	**0,88**	0,09	**1.14**
Pancreas	**1,13**	0,09	**1.27**
Pituitary gland	**0,92**	0,09	**1.19**
Prostate	**1,98**	0,44	**1.90**
Rectosigmoid colon wall	**1,42**	0,27	**1.20**
Red marrow	**1,12**	0,12	**1.09**
Right colon wall	**0,97**	0,08	**0.99**
SI wall	**1,08**	0,12	**1.07**
Salivary glands	**0,83**	0,08	**1.15**
Skin	**0,72**	0,07	**0.89**
Spleen	**1,50**	0,24	**1.32**
Stomach wall	**0,87**	0,08	**0.98**
Systemic lymph nodes	**1,13**	0,12	**1.35**
Testes	**1,00**	0,11	**1.24**
Thoracic lymph nodes	**0,95**	0,09	**1.22**
Thymus	**0,89**	0,09	**1.17**
Thyroid	**0,87**	0,08	**1.12**
Tongue	**0,63**	0,07	**0.71**
Tonsils	**0,94**	0,09	**1.21**
Ureters	**1,40**	0,16	**1.45**
Urinary bladder wall	**3,41**	1,06	**4.66**
ED ICRP 103	**1,19**	0,13	**1.40**
ED ICRP 60	**1,11**	0,11	**1.27**